Eur Biophys J (2011) 40:715–726
DOI 10.1007/s00249-011-0684-5

ORIGINAL PAPER

Molecular dynamics simulation of mammalian 15S-lipoxygenase with AMBER force field

Syed Tarique Moin · Thomas S. Hofer · Rabia Sattar · Zaheer Ul-Haq

Received: 4 November 2010 / Revised: 28 November 2010 / Accepted: 4 February 2011 / Published online: 1 March 2011

Abstract A molecular dynamics simulation study of mononuclear iron 15S-lipoxygenase (15S-LOX) from rabbit reticulocytes was performed to investigate its structure and dynamics; newly developed AMBER force field parameters were employed for the first coordination sphere of the catalytic iron (II). The results obtained from this study demonstrate that the structural features of the catalytic iron coordination site are in good agreement with available data obtained from experiments. The motional flexibility of the N-terminal β-barrel domain is greater than the C-terminal catalytic domain; flexibility was assessed in terms of *B*-factors and secondary structure calculations. The significant features obtained for the relative motional flexibility of these two domains of 15S-LOX in solution as well as the isolated C-terminal domain were analyzed in terms of radius of gyration and maximum diameter, which correlated well with the structural flexibility of 15-lipoxygenase-1 in solution as probed by small-angle X-ray scattering. The motional flexibility indicates interdomain motion between the N-terminal β-barrel and the C-terminal catalytic domain; this was further verified by the evaluation of central bending in the solvated LOX molecule, which identified an unstructured stretch of amino acids as the interdomain linker. The average bending angle confirmed significant central bending between these two domains, which was linked to the high degree of motional freedom of the N-terminal β-barrel domain in aqueous solutions. This can be considered to have biological relevance for membrane binding as well as for regulating the catalytic domain.

Keywords 15S-lipoxygenase · AMBER force field parameterization · Molecular dynamics simulation · RMSD · Radius of gyration · Motional flexibility and interdomain motion

Introduction

Lipoxygenases (LOXs) belong to a class of dioxygenases containing mononuclear non-heme iron in their active site. LOXs occur throughout the plant and animal kingdoms (Kühn and Thiele 1999; Oliw 2002; Liavonchanka and Feussner 2006) and catalyze the regioselective and stereospecific hydroperoxidation of polyunsaturated essential fatty acids by the addition of molecular oxygen to natural substrates containing (Z,Z)-1,4 pentadiene (Siedow 1991; Ford-Hutchinson et al. 1994; Kühn and Borngräber 1999; Brash 1999). In plants, LOXs are involved in germination and senescence phenomena, acting on their natural substrates, linoleic and linolenic acids (Liavonchanka and Feussner 2006). Mammalian LOXs are derived on the basis of their positional and stereospecificity in the peroxidation of arachidonic acid substrate (Funk 2001), determined by the shape and depth of the cavity as well as the nature of the substrate (Borngräber et al. 1999; Kühn 2000;

Electronic supplementary material The online version of this article (doi:10.1007/s00249-011-0684-5) contains supplementary material, which is available to authorized users.

S. T. Moin · R. Sattar · Z. Ul-Haq (✉)
Dr. Panjwani Center for Molecular Medicine and Drug Research, International Center for Chemical and Biological Sciences, University of Karachi, Karachi 75270, Pakistan
e-mail: zaheer.qasmi@iccs.edu

S. T. Moin · T. S. Hofer (✉)
Theoretical Chemistry Division, Institute of General, Inorganic and Theoretical Chemistry, University of Innsbruck, Innrain 52a, 6020 Innsbruck, Austria
e-mail: t.hofer@uibk.ac.at

Coffa et al. 2005). Furthermore, they produce hydroperoxyeicosatetraenoic acids (HETEs), precursors of critical mediators such as leukotrienes and lipoxins, which play major roles in inflammatory events of arthritis, allergic asthma, and cancer (Hamerman 2005; Samuelsson et al. 1987; Kuhn et al. 2002; Serhan 2004). They are also involved in the synthesis of prostaglandins and thromboxanes. The oxidation of low density proteins (LDLs) by mammalian 15S-LOX produces a number of products linked to the pathogenesis of atherosclerosis (Steinberg et al. 1989). Consequently, mammalian LOXs are potential targets for drugs due to their key roles in the synthesis of inflammatory mediators.

Crystal structures of soybean LOX-L1 (Minor et al. 1996) and LOX-L3 (Skrzypczak-Jankun et al. 1997) and their isoforms VLX-B and VLX-D (Youn et al. 2006), rabbit 15S-LOX1 (Gillmor et al. 1997), and coral 8R-LOX (Oldham et al. 2005) have been resolved and have aided in assessing the properties and molecular basis of this class of protein. All LOXs are folded in two domain structures (Sigal et al. 1988) comprised of a smaller N-terminal β-barrel and a larger C-terminal α-helical catalytic domain. The catalytic domain contains the mononuclear non-heme iron, essential for LOX activity, deeply buried in a cavity within the helical bundle. The first crystal structure of mammalian lipoxygenase in the resting form, that of rabbit 15-LOX with a bound inhibitor (PDB ID: 1LOX), was reported by Gillmor et al. (1997). It was the only lipoxygenase crystal structure that played an important role in clarifying the specificity of various mammalian LOXs and aided in rational design of new inhibitors.

The active site of 15S-LOX consists of a ferrous ion (inactive or resting form) liganded to conserved histidines (His-361, His-366, His-541) and to the carboxylate group of isoleucine (Ile-663) plus an additional histidine (His-545) as expected from sequence alignments (Bertini et al. 2001). The topology of the active site corresponds to a distorted octahedron (see Fig. 1a), and a number of studies have been carried out to elucidate the geometry of active sites in LOXs and to explore the underlying reaction mechanisms. Near-infrared circular dichroism (CD) and magnetic circular dichroism (MCD) techniques have been used to investigate electronic structures of the resting ferrous form of 15-LOX (Pavlosky et al. 1995; Holman et al. 1998). The geometric structures of the LOX active sites were studied for models of ferrous (inactive form) and ferric (active form) active sites via first-principles calculations (Borowski et al. 2001). These studies have shown that the active site of 15-LOX is in six-coordinated form. Choi et al. (2008) has reinterpreted the original mammalian 15S-LOX crystallographic data and elucidated two different conformations of the molecule: the first contains an inhibitor, while the second does not. These two different

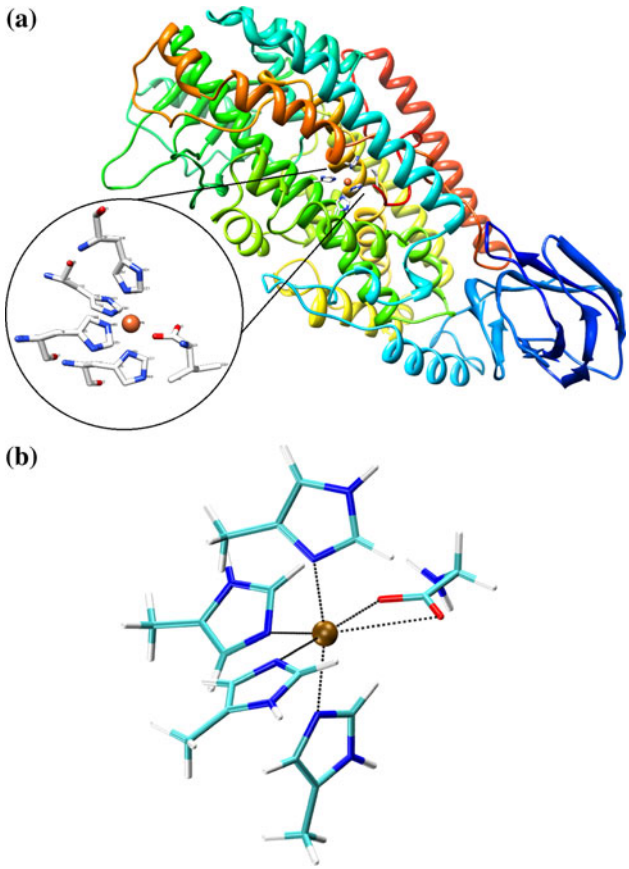

Fig. 1 **a** Structural model of the LOX protein with its active site (*top*) and **b** truncated model of the active site (*bottom*)

conformations correspond to closed and open forms, respectively, and were observed mainly due to the difference in the shape of their substrate binding cavities. The distinct structural characteristics of these cavities are related to the major structural difference in the three spatially adjacent segments: segment I (residues 167–199), segment II (residues 205–215), and segment III (residues 592–604). Segment I includes an α2 helix (residues 177–187) which shows the greater structural changes that can be attributed to the maximum $C_\alpha \ldots C_\alpha$ distances (between equivalent residues of open and closed form of LOX) of 16.0 Å for Asn-190. The α2 helices separated by 12.0 Å have seven (Leu-168 to Ile-194) and five (Phe-175 to Asn-193) turns in the open and closed forms of LOX, respectively. The difference in the number of turns indicates the conformational change from open to closed form, which can be conceived as occurring by unfolding residues Phe-167 to Asp-174. Consequently, this unfolding causes extension of the chain of Asn-193 to Lys-199 amino acid residues, which results in swinging the α2 towards the open space. Similarly, segments II and III are also affected by segment I, and these segments are thus considered critical for shaping the substrate binding cavity. Protein crystal

structures serve key roles in understanding the specificity of enzymes and help in rational design of inhibitors. A solution structure of the ligand-free rabbit 15-lipoxygenase has also been reported to probe the structural flexibility of the N-terminal β-barrel domain by small-angle X-ray scattering. Furthermore, a wide range of other important problems related to biology and biochemistry are linked to structural and dynamic properties of proteins. Molecular dynamics (MD) simulations are considered a worthwhile alternative for studying structural and dynamic properties of biomolecular systems at the atomic level (Karplus and McCammon 2002; Mulholland 2008).

A severe challenge in the treatment of metalloproteins is the construction of reliable potential functions for the metal-protein interaction. The main problem is generally related to the presence of a metal coordinated to several amino acids forming the active site, which imposes restrictions when investigating structure and dynamics. There are no direct structural data available for the LOX/substrate complexes, and there is also an ambiguity found for a water molecule to be a sixth ligand. Force field parameters related to a hydroxyl group analogous to water coordinating to Fe(III) ion as the sixth ligand forming an octahedral geometry have been reported (Saam et al. 2007), and now new AMBER force field parameters have been developed employing only the amino acid residues coordinating to Fe(II) ion in a distorted octahedral geometry (see the Electronic supplementary material). Although knowledge of the crystal structure of 15S-LOX from rabbit reticulocyte provides some insight about the active site geometry, a number of ambiguities remain to be resolved. In this study, the equilibrium structure of the protein in the aqueous environment was obtained by constructing a structural model of fully solvated LOX via molecular mechanical molecular dynamics (MM-MD) simulation of the open form of 15S-LOX (PDB ID: 2P0M, chain A) (Choi et al. 2008) to determine the structure and dynamics of the protein in solution.

Methods

Model of the active site

The crystal structure of 15S-LOX (Choi et al. 2008) has two protein molecules in the asymmetric unit, one with an inhibitor (RS7) and other without, corresponding to closed and open forms, respectively. The open form of the 15S-LOX crystal structure without the inhibitor has been resolved, revealing three histidines (His-361, His-366, and His-541) coordinated to the iron atom via their ε-N atoms, while His-545 and the C-terminal iso-leucine (Ile-663) are bound via the δ-N atom and oxygen atoms of the carboxylate group, respectively. These amino acids constitute the first coordination sphere, and a water molecule is found at a distance of 5.3 Å. The active site model was built using the crystal structure of the open form of 15S-LOX to construct the force field parameters of the active site containing the Fe(II) ion. Figure 1b depicts the truncated structure that corresponds to the active site of 15-S LOX. Amino acids in the iron first coordination sphere were truncated to their most relevant parts; histidines and isoleucine are represented by methyl imidazole rings and glycine, respectively.

Parameterization of the active site iron cluster

In order to derive the force field parameters for the active site of LOX containing iron(II), a bonded model approach was applied as described by Hoops et al. (1991). The protocols for the force field parameterization were outlined by Fox and Kollman (1998) to sustain the compatibility with the AMBER force field for the surrounding protein, as this procedure has been successfully applied for other metalloenzymes in the past (Lin and Wang 2010). The constructed active site model (iron cluster) was subjected to a quantum mechanical constrained geometry optimization utilizing Gaussian03 (Frisch et al. 2009). The B3LYP/6-31G(d,p) level was employed for non-metal atoms and the Fe(II) ion. After the constrained geometry optimization of the iron cluster, equilibrium bond lengths and angles involving the Fe(II) ion and coordinating atoms of the amino acids were obtained. Stretching force constants and bending force constants relevant to their bond lengths and angles were calculated by performing a normal mode analysis on the optimized model. The force constants were calculated analytically in their internal coordinates from diagonal elements of the Hessian matrix. The torsional force constants associated with the Fe(II) ion and the interacting amino acid atoms were considered to be zero as reported by Hoops et al. (1991), based on the rationale that the geometry involving metal ions is rigid and devoid of any significant torsional rotation. Atomic charges were derived by carrying out an electrostatic surface potential (ESP) employing the Merz-Kollman scheme (MK) (Singh and Kollman 1984) for the whole active site containing the Fe(II) ion. To treat electrostatic interactions uniformly, a restrained ESP (RESP) analysis (Bayly et al. 1993; Wang et al. 2000) was performed to derive atomic partial charges. RESP charges exhibit less variation than the standard ESP charges resulting from the Merz-Kollman method, since they are based on the principle that charges of heavy atoms are restrained to an optimal value of zero. The partial atomic charges were derived using electrostatic potential-related charges (Singh and Kollman 1984) for the whole active site extracted from the crystal structure of 15S-LOX

(cf. Fig. 1). In this parameterization scheme, the magnitude of partial charges derived from fitting a classical Coulomb model to quantum mechanical molecular electrostatic potentials (ESP charges) may be attenuated through the use of a restraint function known as RESP charges, which has been proposed for the AMBER force field. These RESP charges of the active site iron complex are then appropriately integrated into the whole RESP charge scheme of the rest of the protein to ensure compatibility. The van der Waals parameters for Fe(II) were set to 0.2 kcal/mol and 2.0 Å, respectively, while standard AMBER atom types were utilized for coordinating amino acid residues in the active site model.

Molecular dynamics simulation protocol

The modified ff03 AMBER force field (Duan et al. 2003) for the protein was applied, and the protonation states for histidines were assigned manually. Missing atoms of the proteins were added by using the xLEaP module of AMBER 10 (Case et al. 2008). The protein was neutralized by adding 5 Na^{+1} as counter-ions, and the system was solvated in a periodic box of 64245 TIP3P (Mark and Nilsson 2001) water molecules extending at least 25.0 Å from each atom of the protein.

To remove bad intra- and intermolecular contacts, energy minimizations followed by equilibrations were carried out using the SANDER module implemented in AMBER 10 prior to the sampling periods. Minimization consisted of 3,000 steps in total, including 1,000 steps of initial minimization of water molecules, keeping only the protein fixed by using position restraints with a force constant of 25 kcal mol^{-1} $Å^{-2}$. Afterwards 1,000 minimization steps were carried out by gradually removing the restraints every 200 steps, and the final stage of the minimization involved the entire system without the application of any restraints. The resulting minimized structures were employed as starting configuration for the MD simulation. The SHAKE algorithm (Ryckaert et al. 1977) was employed to treat all bonds involving hydrogen as rigid, enabling a time step of 2.0 fs. Long-range electrostatic interactions were treated by the particle mesh Ewald algorithm (Essmann et al. 1995), and a cutoff of 8.0 Å was used for non-bonded interactions. The temperature was maintained at 298 K employing the Berendsen thermostat (Berendsen et al. 1984), and a pressure coupling algorithm was used with a relaxation time of 1.0 ps to control the pressure at 1 atm. The system was heated from 50 to 300 K for 50 ps prior to equilibration, and data sampling of the trajectories was performed every picosecond for a total simulation time of 10 ns. The NPT ensemble with periodic boundary condition was applied for the course of the whole simulation. For the analysis and visualization of the trajectories with graphical representation, PTRAJ included in AMBER 10 (Case et al. 2008) and VMD (Humphrey et al. 1996) were used, respectively.

Results and discussion

Force field parameterization of the mononuclear non-heme iron cluster

The geometry optimization of the iron cluster corresponding to the active site of LOX was carried out in light of the previous experimental (Gillmor et al. 1997; Choi et al. 2008; Kuban et al. 1998; Pavlosky et al. 1995; Holman et al. 1998) and theoretical studies (Saam et al. 2007; Borowski et al. 2001; Borowski and Broclawik 2003; Lehnert and Solomon 2003). As mentioned previously, the active site of LOX contains an Fe(II) ion and forms a distorted octahedral structure including a water molecule associated with the second shell at a distance of 5.3 Å from the Fe(II) ion according to X-ray crystallographic data of LOX (Choi et al. 2008). This indicates that the carboxylate of Ile-663 may act as a bidentate ligand, coordinating with both of its oxygens to the Fe(II) ion. The role of the water molecule in the active site geometry was explored from data obtained during simulation. The optimized structure of the iron cluster corresponding to the active site of LOX yielded an appropriate geometry comparable to the observable metallo active site of LOX (cf. Fig. 1b). A variation in the charges of all atoms surrounding the Fe(II) ion was observed. The latter showed a decrease in the atomic charge from +2e to about +0.4e due to electronic distribution between Fe(II) ion and active site residues. The carboxylate oxygens of Ile-663 coordinated directly to Fe(II) ion have negative formal charges, and the atomic charges of the coordinating atoms of histidines range from positive to negative values.

Molecular dynamics simulations

The structure of the metal-containing active site was observed to be stable, which is reflected by the small root mean square deviation (RMSD) of ~0.5 Å for the heavy atoms of the LOX active site residues throughout the whole simulation (cf. Fig. 2). To evaluate the dynamics of the Fe(II) active site, the distance between the Fe(II) ion and all coordinating atoms was monitored during the simulation time for both forms of LOX (see Table 1), and the variation in these distances was compared: the average Fe(II)–N_{ε} distances of His-361, His-366, and His-541 are 2.10, 2.20, and 2.43 Å, respectively, while the distance between the N_{δ} of His-545 and the Fe(II) ion was 2.07 Å, and the carboxylate oxygen atoms of Ile-663 were found at mean distances of 2.09 and 3.22 Å. The structure of the

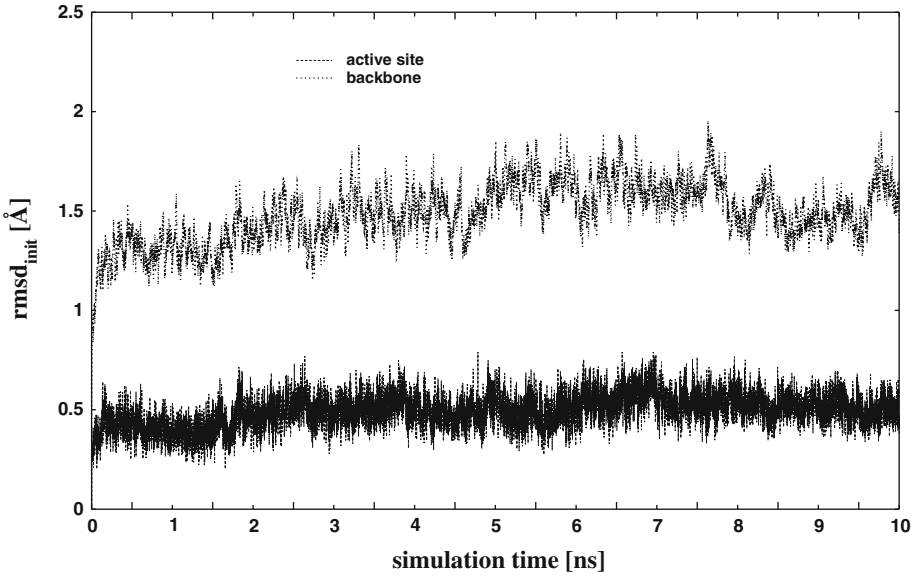

Fig. 2 Time dependence of the root mean square deviation from the initial structure of the simulation ($rmsd_{init}$) for backbone atoms of LOX (*black dotted*) and for heavy atoms of the LOX active site residues (*black dashed*)

Table 1 Binding distances of the ligand directly bound to the Fe(II) ion. Mean values are presented along with fluctuations for the MD simulation and EXAFS data, and values for the rabbit 15S-LOX obtained from X-ray crystallography

Bond distances (Å)	X-ray crystallography (Gillmor et al. 1997; Choi et al. 2008)		EXAFS data[a] (solution) (Kuban et al. 1998)	MD simulation
	1LOX	2P0M		
Fe… ε–$N_{His-361}$	2.08	2.20	2.13	2.10 ± 0.50
Fe… ε–$N_{His-366}$	2.17	2.42	2.13	2.20 ± 0.35
Fe… ε–$N_{His-541}$	2.22	2.35	2.36	2.43 ± 0.52
Fe… δ–$N_{His-545}$	2.28	2.29	2.93	2.07 ± 0.63
Fe…$OXT_{Ile-663}$	2.30	2.16	1.89	2.09 ± 0.34
Fe…$O_{Ile-663}$	2.86	3.22	–	3.22 ± 0.34
Fe…O_{WAT}	–	5.29[b]	2.42	3.70

[a] Extended X-ray absorption fine structure

[b] Minimum distance at which water molecule is found

iron complex corresponds to a distorted octahedron. Along with the distances, the geometry was also analyzed in terms of angle variations evaluated for each angle involving the Fe(II) ion and its coordinating atoms (data not shown). These results are in good agreement with experimental data available for the active site geometry (Gillmor et al. 1997; Choi et al. 2008; Kuban et al. 1998).

In addition, the stability of the overall LOX structure throughout the simulation was investigated via root mean square deviations of backbone atoms with respect to the equilibrated structure to start production dynamics ($rmsd_{init}$) as shown in Fig. 2. The $rmsd_{init}$ showed fluctuations ranging from 1.1 to 1.9 Å, thus confirming a flexibility of the protein structure. The root mean square deviations with respect to the X-ray structure ($rmsd_{X\text{-}ray}$) of all the heavy atoms of LOX were evaluated as well (see Fig. 3). The $rmsd_{X\text{-}ray}$ fluctuated between 1.3 and 2.3 with an average value of 2.0 Å, thus showing no significant structural deviation from the X-ray structure.

The role of the water molecule in the coordination site of the Fe(II) ion present in the active site of mammalian LOX has always been of interest because very few experimental data have been reported so far. The recently determined crystal structure of 15S-LOX (Choi et al. 2008) without inhibitor yields information about a water molecule found at a minimum distance of 5.3 Å; this is in contrast to data on the solution structure of 15-LOX probed by EXAFS (Kuban et al. 1998). The water molecule is believed to play an important role in the catalytic mechanism of LOX in its active Fe(III) form. It was reported that the active site of mammalian LOX is six-coordinated in both ferrous and ferric forms, in contrast to soybean lipoxygenase (SLOX-1), which shows a significant coordination flexibility at the iron site (approximately 40:60%

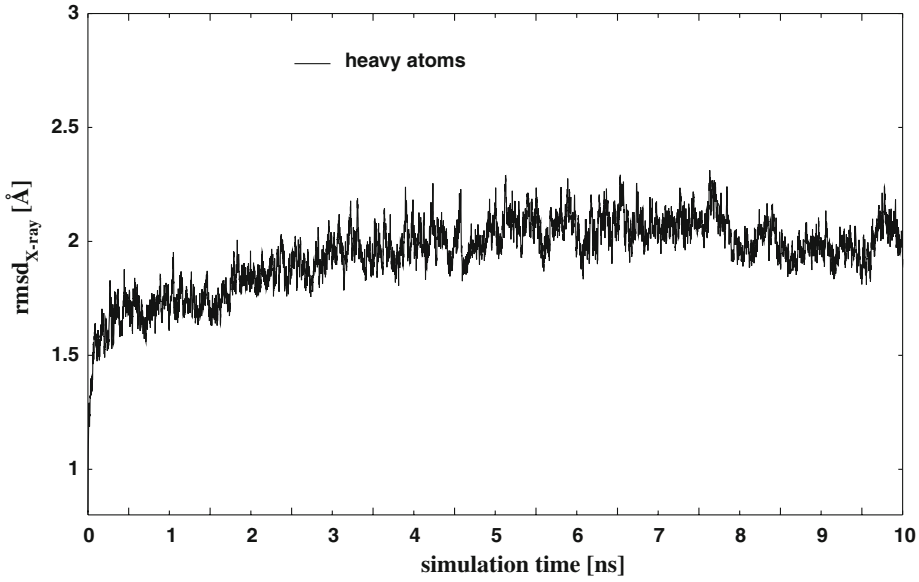

Fig. 3 Time dependence of the root mean square deviation from the X-ray crystal structure ($rmsd_{X\text{-}ray}$) for heavy atoms of the entire LOX protein

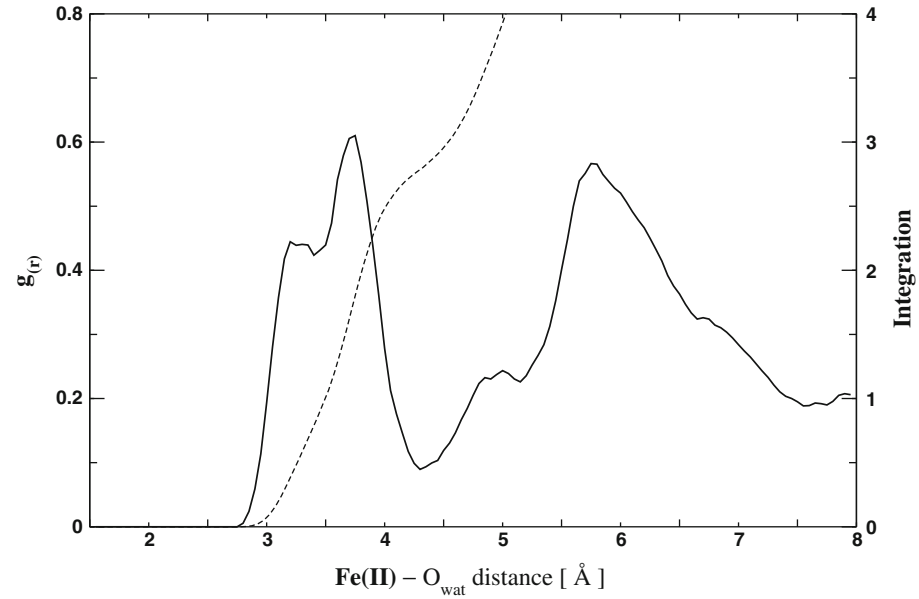

Fig. 4 Radial distribution function between Fe(II) ion and oxygen atoms of water molecules

mixture of five- and six-coordinated species) and which, upon addition of substrate in the anaerobic condition, shifts to the six-coordinated form (Holman et al. 1998). Therefore, the presence of the water molecule in the coordination structure of the iron site was explored via the radial distribution function (RDF) evaluated for the Fe(II) ion and oxygen atoms of water molecules depicted in Fig. 4. The Fe(II)–O_{wat} RDF plot shows a broad peak between 2.7 and 4.3 Å with a mean distance of 3.7 Å. Integration of the RDF up to the minimum at 4.3 Å corresponds to $\sim$1 water molecule bound to Fe(II), which corresponds to a distorted octahedral coordination structure of the iron-containing active site. The presence of a water molecule at a mean distance of 3.7 Å observed during the simulation corresponds to the Fe(II)–$O_{inhibitor}$ distance (3.8 Å) identified via X-ray crystallography (Gillmor et al. 1997) in which the carboxylate oxygen of the inhibitor was believed to replace the water molecule upon formation of the protein-inhibitor complex. In contrast, in the re-interpreted structure, the Fe(II)–$O_{inhibitor}$ distance was found to be 5.3 Å provided that the inhibitor had a planar structure (Choi et al. 2008).

The variation in the flexibility of the LOX structure was further investigated by employing the *B*-factors (B_i) for each C_α atom according to the relationship:

$$B_i = \frac{8}{3}\pi^2\langle\Delta r_i\rangle^2 \quad (1)$$

where $\langle\Delta r_i\rangle$ represents the root mean square fluctuation (rmsf) of the C_α atom of each residue *i*. Figure 5 depicts the calculated *B*-factors that show significant fluctuations in

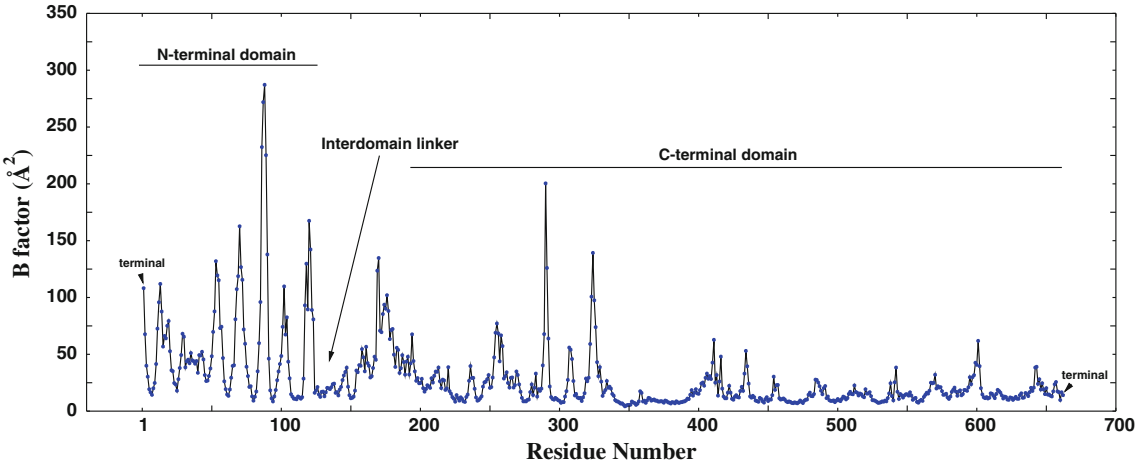

Fig. 5 Calculated *B*-factors of the C_α atoms, averaged over the whole simulation

different regions of LOX. The average B-factor of LOX was observed to be 28.9 Å^2, which was lower than the crystallographic *B*-factors (46.8 Å^2) (Choi et al. 2008) resulting from a higher degree of hydration in the simulation compared to the crystal. The electron density for the atomic coordinates of residues 177–188 in the superficial α2 helix was absent in the PDB structure (1LOX), which was considered disordered (Choi et al. 2008). However, the calculated *B*-factors for these residues indicate a lower flexibility consistent with the electron density obtained for the re-interpreted LOX structure (Choi et al. 2008). Similarly, the surface residues 210–211 and 601–602 demonstrate a reduced flexibility as indicated by the *B*-factors. Each domain of LOX exhibited different dynamics as illustrated by the respective *B*-factors: amino acids in the N-terminal β-barrel have, on average, higher *B*-factors than amino acids in the C-terminal domain. In detail, several segments of N-terminal β-barrel residues as well as the chains connecting to α2 show large *B*-factors (larger than 60 Å^2) consistent with the experimental data obtained from crystallography for the open form of 15S-LOX (Choi et al. 2008). Conversely, the average *B*-factor for the C-terminal catalytic domain was calculated as 20.4 Å, which indicates a low motional flexibility. Besides the differences between the N-terminal and C-terminal domains, the overall active site dynamics of LOX also depends upon different segments as described earlier, in particular segment I, which contains α2 playing an important role in the active site dynamics. The *B*-factor of segment I indicates its conformational flexibility, which is also correlated with the dynamics of segments II and III. Segment III, which contains an α18 helix beneath α2 and the following chain of residues (Arg-599 to Ile-603), also has large dynamics flexibility indicated by its high *B*-factor value. These changes in the structure can in turn influence the segment II residues as well. Strictly in terms of their flexibility, the swinging helices—in particular α2, which has considerable influence in the substrate binding cavity of the protein—also corroborate the secondary structure calculation of the protein as being dominated by different α helices throughout the simulation time (see Fig. 6). To explore the conformational modifications occurring from open to closed form in detail, the dynamics of the protein-substrate complex will be needed. This will result in some limitations when attempting to make substantial comparison between the dynamics of the open and closed forms, in particular these segments associated with the active site of LOX. The dynamics of different regions and segments in LOX, as described by *B*-factors, will be of great consequence for understanding the dynamics of the substrate binding cavity, which is able to accommodate substrates of varying size and nature.

The analysis of the secondary structure of LOX was carried out to assess the stability of amino acid residues in each domain and specifically to assign secondary structure motifs, such as in α-helix, β-strand, random coil, and others along the trajectories. Figure 6 shows that the N-terminal β-barrel domain (amino acid residues 1–110) mostly exists in a stable extended sheet conformation, i.e., in the form of anti-parallel β sheets along with the turns and coils that connect these. Both domains are interconnected via an unstructured stretch (amino acid residues 111–124) that was found to be randomly coiled during the entire simulation with indication of a helix formation for those residues connected to the C-terminal domain. Amino acid residues of the C-terminal domain exhibited variation in their secondary structure to a larger extent than the N-terminal domain. The main feature of the C-terminal catalytic domain is its core region containing two long central helices, which adopt π-helix conformation for four amino acid residues (His 361, 366, 541, and 545) coordinating to the catalytic Fe(II) ion. The secondary structure calculation

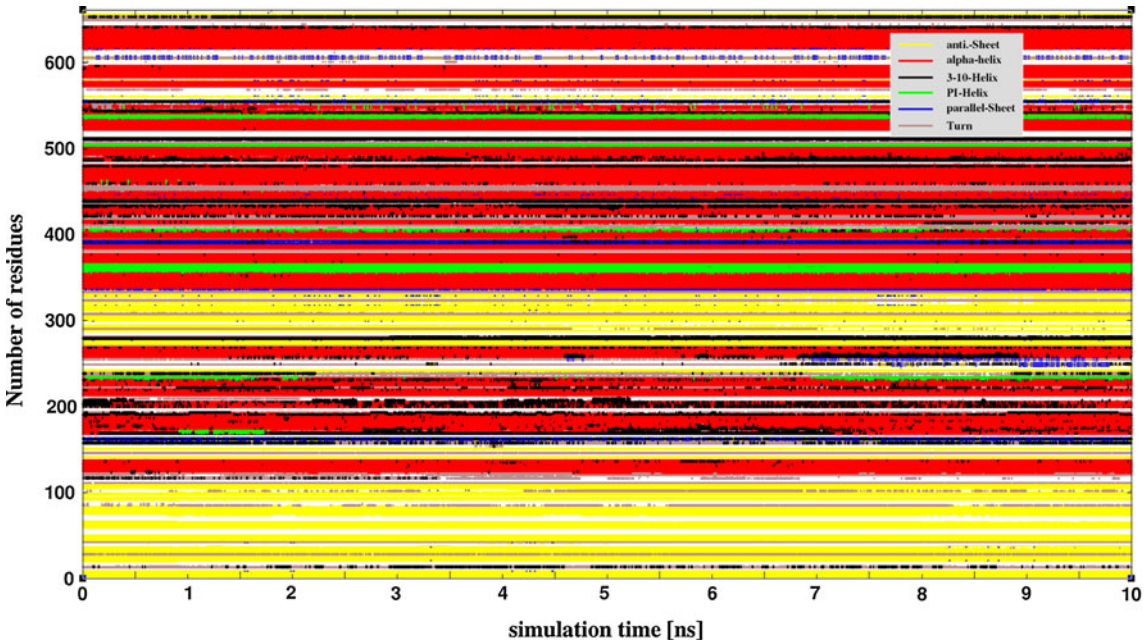

Fig. 6 Secondary structure evaluation as a function of the simulation time evaluated for the entire 15S-LOX

also exhibits a similar trend for these residues of the core region, attributed to the π-helical structure throughout the simulation time. Besides this core region, conformational changes in the overall substrate binding cavity of the 15S-LOX are also significant. The amino acids forming the cavity are located in stabilized conformations composed of helices and loops such as α22, α9–α10, and others.

To further verify the conclusions about the motional flexibility drawn from *B*-factors of the residues of each domain, the time evolution of the radius of gyration (R_g) of the entire protein and the C-terminal domain alone were analyzed as shown in Fig. 7. The average value of R_g for the entire protein in solution was found to be 28.1 ± 0.3 Å (see. Fig. 7a), which is lower than the experimental value of 33.4 ± 0.5 Å for the solution structure of ligand-free rabbit 15-lipoxygenase-1 found by small-angle X-ray scattering (SAXS) (Hammel et al. 2004), thus indicating that these domains exist in a tight unit and interact with each other. The molecular volume of the entire LOX in solution was also calculated in terms of the maximum diameter (D_{max}) (inset: Fig. 7a). An average value of 107 ± 5 Å was obtained, which is also lower than the value obtained by SAXS (135 ± 7 Å), but suggests an extended structure of the protein in solution compared to the crystal structure of 15-LOX, which had a D_{max} value of 100 Å. The deviation between theoretical and experimental (R_g and D_{max}) values may be due to physico-chemical and physiological conditions employed in the experimental studies. The most likely explanation for the difference between the solution and crystal structures of LOX would be the higher motional flexibility of the N-terminal β-barrel domain compared to the C-terminal catalytic domain, as the former has a high temperature factor (Choi et al. 2008). The high degree of flexibility of the N-terminal β-barrel domain is further supported by the R_g and D_{max} values evaluated for the extracted C-terminal catalytic domain comprised of residues 115–662 during the simulation shown in Fig. 7b. The average R_g and D_{max} values were calculated as 24.7 ± 0.3 and 98.7 ± 7 Å, which are comparable to the SAXS experimental data (R_g = 26.2 ± 1.2 and 80 ± 5 Å). The data obtained from the simulation suggest that the structure of the C-terminal domain in solution is similar to that of the crystal structure, and the increased R_g value of the entire LOX in solution compared to the crystal structure results from a higher librational flexibility of the N-terminal β-barrel domain than observed for the C-terminal catalytic domain, leading to interdomain motion. Table 2 summarizes the characteristic parameters of the structural flexibility of 15S-LOX in solution obtained via MD simulation and experiment.

The assumption of interdomain motion of the N-terminal domain of 15S-LOX was further verified by the evaluation of central bending in the solvated LOX molecule by considering the unstructured stretch of amino acids 111–124 (random coil) as an interdomain linker. Therefore, it was considered worthwhile to explore such motion within the 10 ns simulation. It was decided to examine the time dependence of central bending, calculated as the angle from the center of mass of the N-terminal β-barrel domain (amino acid residues 1–110) to the center of mass of the interdomain linker (amino acid residues 111–124) to the center of mass of the C-terminal catalytic domain (amino

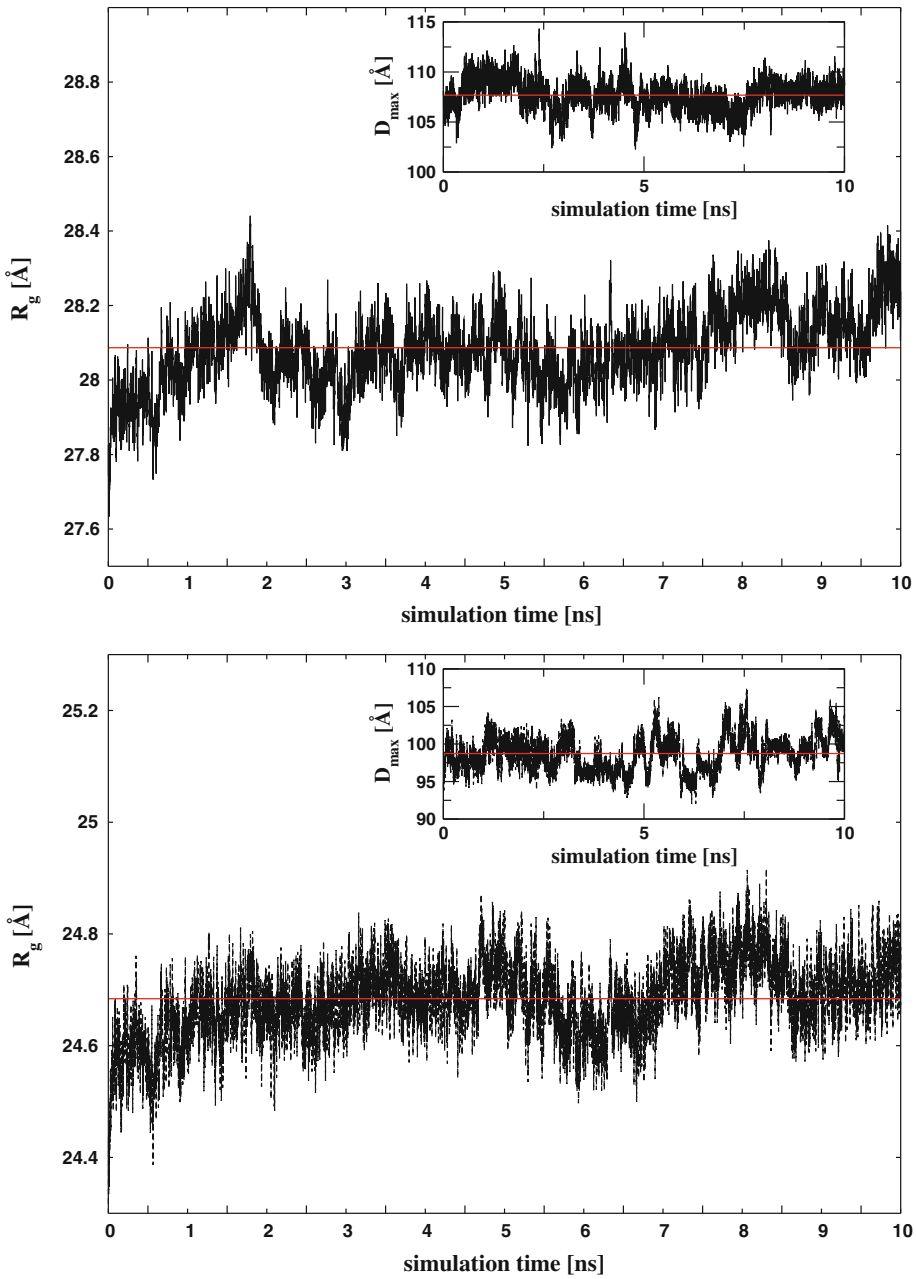

Fig. 7 Radius of gyration (R_g) of the backbone and sidechain elements for the entire 15S-LOX (*top*) and isolated C-terminal catalytic domain in solutions as a function of time (*bottom*). *Insets* Variation of maximum diameter (D_{max}) of entire LOX and C-terminal domain during simulation

Table 2 Characteristic parameters of the structural flexibility of 15S-LOX obtained from MD simulation and a small-angle X-ray scattering experiment

Methods	Entire 15S-LOX		Isolated C-terminal domain	
	R_g(Å)	D_{max} (Å)	R_g (Å)	D_{max} (Å)
MD simulation	28.1 ± 0.3	107 ± 5	24.7 ± 0.3	98.7 ± 7
SAXS experiment (Hammel et al. 2004)	33.4 ± 0.5	135 ± 7	26.2 ± 1.2	80 ± 5

acid residues 125–662). Figure 8a shows the fluctuation in the central bending of solvated LOX in the range from 80 and 89° with an average value of 84.7° depicted by a histogram, thus indicating that significant bending occurs between the two domains in solution. This is also reflected by the half-width of the bending angle distribution, which was 3.5° (see Fig. 8b). This interdomain movement is linked to a high degree of motional freedom of the N-terminal β-barrel domain in aqueous solutions (Hammel et al. 2004), which can be considered of biological relevance for

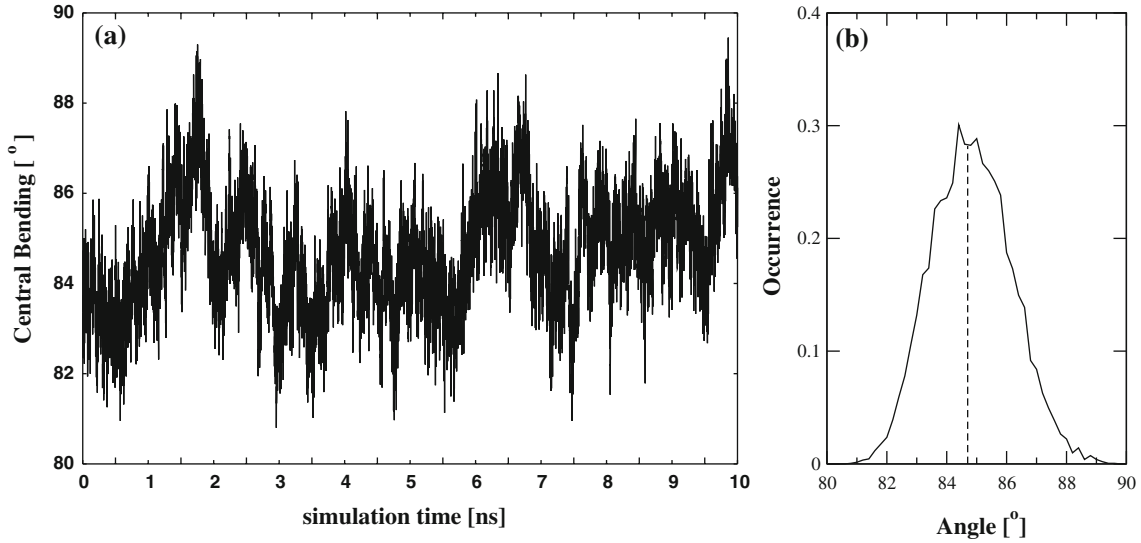

Fig. 8 **a** Time evolution of the bending angle formed between the N-terminal β-barrel and C-terminal catalytic domain of 15S-LOX in solution. **b** Histogram analysis to evaluate the average angle formed during the simulation

membrane binding as well as for regulation of the catalytic domain.

The crystal structure of the mammalian 15-LOX reported by Gillmor et al. (1997) was also solved in the form of an enzyme-inhibitor complex, but it represents an inactive form of the protein. It is conceivable to assume that the structural flexibility of the protein may be impaired by the binding of substrates and/or inhibitors, which prevents a relaxation of the 3D structure. However, the crystallographic structure of 15S-LOX by Choi et al. (2008) includes both forms of the protein, along with complete structural information of those residues that could not be solved in the previous X-ray crystallography study (Gillmor et al. 1997). Therefore, it became easier to explore the structure and dynamics of the mammalian LOX in detail. The functional properties of metalloproteins are mainly associated with the geometric features of the active site, thus the evaluation of an accurate geometry of the iron coordination site in 15-S LOX is of particular importance to establish the structure-function relationship.

Conclusion

Newly developed AMBER force field parameters were successfully applied in a molecular dynamics simulation study investigating the structure and dynamics of 15S-LOX in solution. Due to inhibitor/substrate binding, the structural flexibility of the protein may be impaired, thus preventing the relaxation of the 3D structure. Therefore, to fully explore the structural flexibility of the protein prior to complexation with either a substrate or an inhibitor, the motional flexibility of the N-terminal β-barrel domain, which was found to be larger than that of the C-terminal domain in solution, was evaluated. The motional flexibility was further verified by the central bending of LOX in solution by evaluating the angle formed by the two domains and the linker unit. The overall dynamics showed that the N-terminal β-barrel domain in the LOX plays a regulatory function for either activated or impaired catalysis and membrane binding, since it has a higher degree of librational freedom compared to the catalytic domain. These effects can be further analyzed by evaluating the dynamics of interdomain interaction between the N-terminal β-barrel and the C-terminal domain of LOX in solution, which is beneficial for understanding the allosteric mechanism of catalysis carried out by this enzyme.

Acknowledgments Financial support for this work by the Austrian Science Foundation (FWF) and an Austrian Technology Grant (BMWF/RFTE) for Syed Tarique Moin is gratefully acknowledged.

References

Bayly CI, Cieplak P, Cornell W, Kollman PA (1993) A well-behaved electrostatic potential based method using charge restraints for deriving atomic charges: the RESP model. J Phys Chem 97:10269–10280

Berendsen HJC, Postma JPM, Gunsteren WFV, DiNola A, Haak JR (1984) Molecular dynamics with coupling to an external bath. J Chem Phys 81:3684–3690

Bertini I, Sigel A, Sigel H (2001) Handbook on metalloproteins. CRC Press, New York

Borngräber S, Browner M, Gillmor S, Gerth C, Anton M, Fletterick R, Kühn H (1999) Shape and specificity in mammalian 15-lipoxygenase active site. J Biol Chem 274:37345–37350

Borowski T, Broclawik E (2003) Catalytic reaction mechanism of lipoxygenase. A density functional theory study. J Phys Chem B 107:4639–4646

Borowski T, Krol M, Chruszcz M, Broclawik E (2001) Catalytic reaction mechanism of lipoxygenase. A density functional theory study. J Phys Chem B 105:12212–12220

Brash AR (1999) Lipoxygenases: occurrence, functions, catalysis, and acquisition of substrate. J Biol Chem 274:23679–23682

Case DA, Darden TA, TE Cheatham I, Simmerling CL, Wang J, Duke RE, Luo R, Crowley M, Walker RC, Zhang W, Merz KM, Wang B, Hayik S, Roitberg A, Seabra G, Kolossvry I, Wong KF, Paesani F, Vanicek J, Wu X, Brozell SR. Steinbrecher T, Gohlke H, Yang L, Tan C, Mongan J, Hornak V, Cui G, Mathews DH, Seetin MG, Sagui C, Babin V, Kollman PA (2008) AMBER 10. University of California, San Francisco

Choi J, Chon JK, Kim S, Shin W (2008) Conformational flexibility in mammalian 15S-lipoxygenase: reinterpretation of the crystallographic data. Proteins Struct Funct Bioinf 70:1023–1032

Coffa G, Schneider C, Brash AR (2005) A comprehensive model of positional and stereo control in lipoxygenases. Biochem Biophys Res Commun 338:87–92

Duan Y, Wu C, Chowdhury S, Lee MC, Xiong G, Zhang W, Yang R, Cieplak P, Luo R, Lee T, Caldwell J, Wang J, Kollman P (2003) A point-charge force field for molecular mechanics simulations of proteins based on condensed-phase quantum mechanical calculations. J Comput Chem 24:1999–2012

Essmann U, Perera L, Berkowitz ML, Darden T, Lee H, Pedersen LG (1995) A smooth particle mesh Ewald method. J Chem Phys 103:8577–8593

Ford-Hutchinson AW, Gresser M, Young RN (1994) 5-Lipoxygenase. Annu Rev Biochem 63:383–417

Fox T, Kollman PA (1998) Application of the RESP methodology in the parametrization of organic solvents. J Phys Chem B 102:8070–8079

Frisch MJ, Trucks GW, Schlegel HB, Scuseria GE, Robb MA, Cheeseman JR, Scalmani G, Barone V, Mennucci B, Petersson GA (2009) Gaussian 09, revision A.02. Gaussian, Wallingford, CT

Funk CD (2001) Prostaglandins and leukotrienes: advances in eicosanoid biology. Sci Agric 294:1871–1875

Gillmor SA, Villaseñor A, Fletterick R, Sigal E, Browner MF (1997) The structure of mammalian 15-lipoxygenase reveals similarity to the lipases and the determinants of substrate specificity. Nat Struct Biol 4:1003–1009

Hamerman D (2005) Osteoporosis and atherosclerosis: biological linkages and the emergence of dual-purpose therapies. QJM 98:467–484

Hammel M, Walther M, Prassl R, Kuhn H (2004) Structural flexibility of the N-terminal beta-barrel domain of 15-lipoxygenase-1 probed by small angle X-ray scattering. Functional consequences for activity regulation and membrane binding. J Mol Biol 343:917–929

Holman TR, Zhou J, Solomon EI (1998) Spectroscopic and functional characterization of a ligand coordination mutant of soybean lipoxygenase-1: first coordination sphere analogue of human 15-lipoxygenase. J Am Chem Soc 120:12564–12572

Hoops SC, Anderson KW, Merz KM (1991) Force field design for metalloproteins. J Am Chem Soc 113:8262–8270

Humphrey W, Dalke A, Schulten K (1996) VMD: visual molecular dynamics. J Mol Graphics 14:33–38

Karplus M, McCammon JA (2002) Molecular dynamics simulations of biomolecules. Nat Struct Mol Biol 9:646–652

Kuban RJ, Wiesner R, Rathman J, Veldink G, Nolting H, Solé VA, Kühn H (1998) The iron ligand sphere geometry of mammalian 15-lipoxygenases. Biochem J 332:237–242

Kühn H (2000) Structural basis for the positional specificity of lipoxygenases. Prostaglandins Other Lipid Mediat 62:255–270

Kühn H, Borngräber S (1999) Lipoxygenase and their metabolites. Plenum, New York

Kühn H, Thiele BJ (1999) The diversity of the lipoxygenase family: many sequence data but little information on biological significance. FEBS Lett 449:7–11

Kuhn H, Walther M, Kuban RJ (2002) Mammalian arachidonate 15-lipoxygenases: structure, function, and biological implications. Prostaglandins Other Lipid Mediat 68:263–290

Lehnert N, Solomon EI (2003) Density-functional investigation on the mechanism of H-atom abstraction by lipoxygenase. J Biol Inorg Chem 8:294–305

Liavonchanka A, Feussner I (2006) Lipoxygenases: occurrence, functions and catalysis. J Plant Physiol 163:348–357

Lin F, Wang R (2010) Systematic derivation of AMBER force field parameters applicable to zinc-containing systems. J Chem Theor Comput 6:1852–1870

Mark P, Nilsson L (2001) Structure and dynamics of the TIP3P, SPC, and SPC/E water models at 298 K. J Phys Chem A 105:9954–9960

Minor W, Steczko J, Stec B, Otwinowski Z, Bolin JT, Walter R, Axelrod B (1996) Crystal structure of soybean lipoxygenase L-1 at 1.4 Å resolution. Biochem Cell Biol 35:10687–10701

Mulholland AJ (2008) Introduction. Biomolecular simulation. J R Soc Interface 5:169–172

Oldham ML, Brash AR, Newcomer ME (2005) Insights from the X-ray crystal structure of coral 8R-lipoxygenase: calcium activation via a C2-like domain and a structural basis of product chirality. J Biol Chem 280:39545–39552

Oliw EA (2002) Plant and fungal lipoxygenases. Prostaglandins Other Lipid Mediat 68:313–323

Pavlosky MA, Zhang Y, Westre TE, Gan QF, Pavel EG, Campochiaro C, Hedman B, Hodgson KO, Solomon EI (1995) Near-infrared circular dichroism and magnetic circular dichroism and x-ray absorption spectral comparison of the non-heme ferrous active sites of plant and mammalian 15-lipoxygenases. J Am Chem Soc 117:4316–4327

Ryckaert JP, Ciccotti G, Berendsen HJC (1977) Numerical integration of the Cartesian equations of motion of a system with constraints: molecular dynamics of n-alkanes. J Comput Phys 23:2327–341

Saam J, Ivanov I, Walther M, Holzhütter HG, Kuhn H (2007) Molecular dioxygen enters the active site of 12/15-lipoxygenase via dynamic oxygen access channels. Proc Natl Acad Sci 104:13319–13324

Samuelsson B, Dahlen SE, Lindgren JA, Rouzer CA, Serhan CN (1987) Leukotrienes and lipoxins: structures, biosynthesis, and biological effects. Sci Agric 237:1171–1176

Serhan CN (2004) Clues for new therapeutics in osteoporosis and periodontal disease: new roles for lipoxygenases? Expert Opin Ther Targets 8:643–652

Siedow JN (1991) Plant lipoxygenase: structure and function. Annu Rev Plant Physiol Plant Mol Biol 42:145–188

Sigal E, Craik CS, Highland E, Grunberger D, Costello LL, Dixon RAF, Nadel J (1988) Molecular cloning and primary structure of human 15-lipoxygenase. Biochem Biophys Res Commun 157:457–464

Singh UC, Kollman PA (1984) An approach to computing electrostatic charges for molecules. J Comput Chem 5:129–145

Skrzypczak-Jankun E, Amzel LM, Kroa BA, MO Funk J (1997) Structure of soybean lipoxygenase L3 and a comparison with its L1 isoenzyme. Proteins Struct Funct Bioinf 29:15–31

Steinberg D, Parthasarathy S, Carew TE, Khoo JC, Witztum JL (1989) Beyond cholesterol: modifications of low-density

lipoprotein that increase its atherogenicity. N Engl J Med 320:915–924

Wang J, Cieplak P, Kollman PA (2000) How well does a restrained electrostatic potential (RESP) model perform in calculating conformational energies of organic and biological molecules? J Comput Chem 21:1049–1074

Youn B, Sellhorn GE, Mirchel RJ, Gaffney BJ, Grimes HD, Kang CH (2006) Crystal structures of vegetative soybean lipoxygenase VLX-B and VLX-D, and comparisons with seed isoforms LOX-1 and LOX-3. Proteins Struct Funct Bioinf 65:1008–1020